Pre-print version. Published in Earthquake Engng Struct Dyn. 50(1): 99-115, Wiley, 2021.

PHYSICS-BASED PROBABILISTIC SEISMIC HAZARD AND LOSS ASSESSMENT IN LARGE URBAN AREAS: A SIMPLIFIED APPLICATION TO ISTANBUL

Marco Stupazzini[1], Maria Infantino[2], Alexander Allmann[1], and Roberto Paolucci[2]

[1]Munich Re, Munich, Germany

[2]Department of Civil and Environmental Engineering, Politecnico di Milano, Italy

A set of 3D physics-based numerical simulations (PBS) of possible earthquakes scenarios in Istanbul along the North Anatolian Fault (Turkey) is considered in this paper to provide a comprehensive example of application of PBS to probabilistic seismic hazard (PSHA) and loss assessment in a large urban area. To cope with the high-frequency (HF) limitations of PBS, numerical results are first post-processed by a recently introduced technique based on Artificial Neural Networks (ANN), providing broadband waveforms with a proper correlation of HF and LF portions of ground motion as well as a proper spatial correlation of peak values also at HF, that is a key feature for the seismic risk application at urban scale. Secondly, before application to PSHA, a statistical analysis of residuals is carried out to ensure that simulated results provide a set of realizations with a realistic within-event and between-event variability of ground motion. PBS results are then applied in a PSHA framework, adopting both the "generalized attenuation function" (GAF) approach, and a novel "footprint" (FP) based approach aiming at a convenient and direct application of PBS into PSHA. PSHA results from both approaches are then compared with those obtained from a more standard application of PSHA with empirical ground motion models. Finally, the probabilistic loss assessment of an extended simplified portfolio of buildings is investigated, comparing the results obtained adopting the different approaches: (i) GMPE, (ii) GAF and (iii) FP. Only FP turned out to have the capability to account for the specific features of source and propagation path, while preserving the proper physically-based spatial correlation characteristics, as required for a reliable loss estimate on a building portfolio spatially distributed over a large urban area.

KEYWORDS

3D Physics based numerical simulations, near-source ground motion, probabilistic seismic hazard assessment, loss estimates of a distributed portfolio of assets.

INTRODUCTION

Being rooted in a PSHA framework [Cornell 1968, Esteva 1967,1968], this paper aims at highlighting the impact of different approaches used to propagate ground motions from the seismic source to the site. On this regard, empirical ground motion prediction equations (GMPEs) and 3D physics-based numerical simulations (PBSs) are generally presented as alternative tools, with basic advantages and limitations as summarized in Table 1. While the use of GMPEs is well consolidated in PSHA, PBSs are gaining popularity thanks to the ongoing progress in recent years, that allowed to validate real earthquake case studies and compare the simulation results with records (e.g. Razafindrakoto et al. 2018, Bradley et al. 2017, Evangelista et al. 2017, Taborda et al 2016, Goulet et al. 2015, Paolucci et al. 2015, Taborda and Bielak 2013, Smerzini and Villani 2012, Guidotti et al. 2011, Pilz et al. 2011). These studies encouraged the use of PBSs for PSHA, with approaches that may roughly be subdivided into two main groups. A first class intends to exploit the PBS results to improve the GMPEs hazard estimations. In this perspective, within the SCEC's CyberShake Project, [Graves et al. 2011] computed an interpolated field of residuals between PBSs and GMPEs predictions and produced the seismic hazard map by adding such residuals to the original GMPE-based hazard map. Furthermore, [Abrahamson and Wooddell 2018] proposed to use 3D simulations to update the nonergodic spatially-varying coefficients of the GMPEs to be used in PSHA.

A second class of research works aims at replacing empirical GMPE by PBS results within site-specific applications of PSHA: on the one hand [Villani et al. 2014], [Hutchings et al. 2007] and [Convertito et al. 2006] replaced the statistical moments from GMPE by those obtained from probability distribution of simulated ground motion, while on the other hand, [Tarbali et al. 2019] and [Stupazzini et al. 2015] directly integrated PBSs results into PSHA without postulating any probability distribution, but simply averaging out of the resulting scenarios. A further advantage of the latter approach is that it may directly incorporate within each ground motion scenario the site specific factors

affecting ground motion at a given site that the 3D numerical simulations allow to account for, such as soil nonlinear behavior [Roten et al. 2017, Taborda et al. 2012], geologic/topographic irregularities, basin effects or complex fault geometry.

Owing to their different nature, the alternative between GMPEs or PBSs as tools to describe ground motion in a PSHA should be driven by the specific features of each case study [Paolucci et al., 2018a]. As a matter of fact, GMPEs find their natural domain of application whenever the tectonic and geologic features governing seismic hazard, as well as the earthquake Magnitude and source-to-site distance, fall within the range for which the GMPE was calibrated. When this is not the case, PBSs may be considered as a valid and rationale alternative, provided that site-specific information is sufficient to constrain a reliable 3D model of the seismic source and of the geology of the area. Validation with local records plays a key role to strengthen the adoption of both GMPEs and PBSs to the specific case study.

With the objective to highlight the impact of seismic hazard and loss assessment by different approaches, either based on GMPEs or PBSs, in this work we will exploit the set of broadband PBS presented in [Infantino et al. 2020] to provide an application to Istanbul within a (re)insurance framework. Indeed, the concern on the high hazard caused by the proximity of Istanbul to the North Anatolian Fault, drove numerous national and international projects aimed both to update the Turkish hazard maps (for a comprehensive review see Akkar et al. 2018), and to improve hazard estimates (e.g. Spagnuolo et al. 2016, Ince 2012, Kalkan et al. 2009, Erdik et al. 2004, Atakan et al. 2002). Moreover, in addition to these GMPE-based studies, examples of seismic hazard and loss assessments from physics-based numerical simulations can be found in [Ansal et al.,2009], who coupled the results of simulated ground motions at bedrock in Istanbul with 1D site-specific amplification studies and in [Mert et al. 2016], who provided physics-based hazard estimates in a limited number of sites.

Table1 Advantages and limitations of GMPEs and PBSs (after [Paolucci et al. 2018a])

	GMPEs	PBSs
Advantages	○ Ease-of-use ○ Calibrated on earthquake records ○ Adapted to different tectonic environments and site conditions	○ Flexibility to produce time histories of simulated ground motions in arbitrary site and source-specific conditions ○ Naturally accounting for the spatial correlation of simulated ground motions ○ Numerical laboratory to gain insight into the earthquake physics and seismic wave propagation phenomena
Limitations	○ Lack of records to constrain important conditions, such as near-source and complex geological environments ○ Only peak values of motion ○ Recalibration when new data are available ○ In most cases, no explicit spatial correlation of ground motion intensities among multiple sites and among different spectral periods	○ High-frequency computational and modelling limit ○ High computational costs ○ Need of expert users ○ Need of spatially extended information to construct a reliable 3D model

The paper is organized as follows. First, the numerical approach is shortly introduced, making reference to [Infantino et al., 2020] for a more comprehensive description. Second, an overview of the ANN-based approach to estimate the short period response spectral ordinates based on the long period values obtained from PBS is introduced, making reference in this case for further details to [Paolucci et al., 2018b]. Before application to PSHA, a statistical analysis of the residuals from the set of PBS is carried out in order to ensure that the simulated results provide a set of realizations of future ground motions in the Istanbul area with a realistic within-event and between-event variability. Subsequently, the PBSs are introduced into a PSHA framework and results critically compared with the outcomes of a conventional GMPE–based PSHA [Cornell 1968, Esteva 1967,1968].

Finally, with the objective to provide a simplified example of application demonstrating the relevance of PBSs in catastrophic risk modelling, the expected loss on an artificial building portfolio distributed over the entire metropolitan region of Istanbul are computed.

OVERVIEW OF THE NUMERICAL APPROACH AND GENERATION OF BROADBAND WAVEFORMS

The numerical approach to obtain broadband PBSs couples a full 3D wave propagation scheme for generating low-frequency waveforms and a method based on the use of Artificial Neural Network (ANN) to enrich the high frequency content. Regarding the former contribution, the low-frequency numerical simulations were carried out using the open-source code SPEED (Spectral Elements in Elastodynamics with Discontinuous Galerkin) which allows to simulate the earthquake rupture and the propagation path from the source to the site including localized geological irregularities and complex fault geometries. For details on the numerical code, the mathematical formulation and main applications, the reader is referred to the relevant publications [Antonietti et al. 2018, Mazzieri et al. 2013] and to the dedicated website (http://speed.mox.polimi.it/). The frequency threshold up to which the PBSs can be considered reliable is mainly related to the level of detail of both the seismic source description and of the information used to setup a 3D soil model. Broadband synthetics, required in several civil engineering applications, are generally obtained coupling in the frequency domain the low-frequency (LF) PBS with the high-frequency (HF) waveforms from stochastic methods, based either on point- or on finite-source modeling (e.g., Motazedian and Atkinson 2005, Boore 2003) or on Empirical Green's functions (e.g., Mai et al. 2010, Kamae et al. 1998). Despite very popular, such a hybrid approach suffers of a twofold drawback which limits its use mainly for regional applications: first, the LF and HF parts of the resulting hybrid broadband waveform may lack correlation, because they are typically obtained by independent numerical approaches; second, while the spatial correlation of LF peak values of ground motion is ensured by the PBS, this may not occur for the HF part, since it is driven by stochastic approaches. For these reasons, we opted for the alternative approach already presented and validated in [Paolucci et al. 2018b], referred to as ANN2BB, which takes advantage of ANN, generally used to estimate the nonlinear relationship between input and output variables for the correlation of which fast- and closed-form rules are not available. In our case the input variables are the LF spectral acceleration (SA) for $T \geq T^*$, where $T^*$is the threshold period corresponding to the range of validity of PBS, while the outputs are the HF SA. The ANN here considered is called multilayer perceptron [Bishop and Roach 1992, Bishop 1995] and consists of a two-layer (i.e., nodes are grouped in layers) feed-forward (i.e., the arcs joining nodes are unidirectional, and there are no cycles) neural network with sigmoid hidden neurons (the so-called activation functions) and a linear output neuron (Figure 1a). The number of nodes in the input N_n^i and output N_n^o layer equals the number of input variables N_{SA}^{LF} and output variables N_{SA}^{SF}, respectively. Once specified the ANN design, the ANN2BB procedure consists of the three main steps sketched in Figure 1, with details provided in [Paolucci et al. 2018b]: (1) the ANN is trained on a strong-motion dataset, to correlate short-period ($T < T^*$) spectral ordinates with the long-period ones ($T \geq T^*$); (2) the trained ANN is used to obtain the short-period spectral ordinates of the physics-based earthquake ground motion for periods below T^* (Figure 1b); and (3) the LF PBS are enriched at high frequencies by an iterative spectral matching procedure, until the response spectrum approaches within a given tolerance the short-period target output of the ANN (Figure 1c).

[Paolucci et al., 2018b] introduced the ANN-based technique taking advantage of a training strong-motion dataset within a limited set of magnitude (from 5 to 7) and distance (up to 30 km), specific to the Italian context of seismic hazard evaluations. Considering the validation test of the 2012 M_w6 Po Plain earthquake, they showed that the treatment of the PBS waveforms by the ANN2BB approach is able to : (i) describe ground shaking spatial variability even at short periods incorporating source and geological effects; (ii) produce realistic time histories and peak ground values consistent with records; (iii) reproduce the spatial correlation structure of the ground motion also in the HF range. Since the range of magnitude and distances considered previously were not sufficiently extended to cope with this application to Istanbul, we decided to train the ANN with the Next Generation Attenuation (NGA)-West2 dataset [Ancheta et al. 2014], covering distances up to 100 km and magnitude up to 7.7.

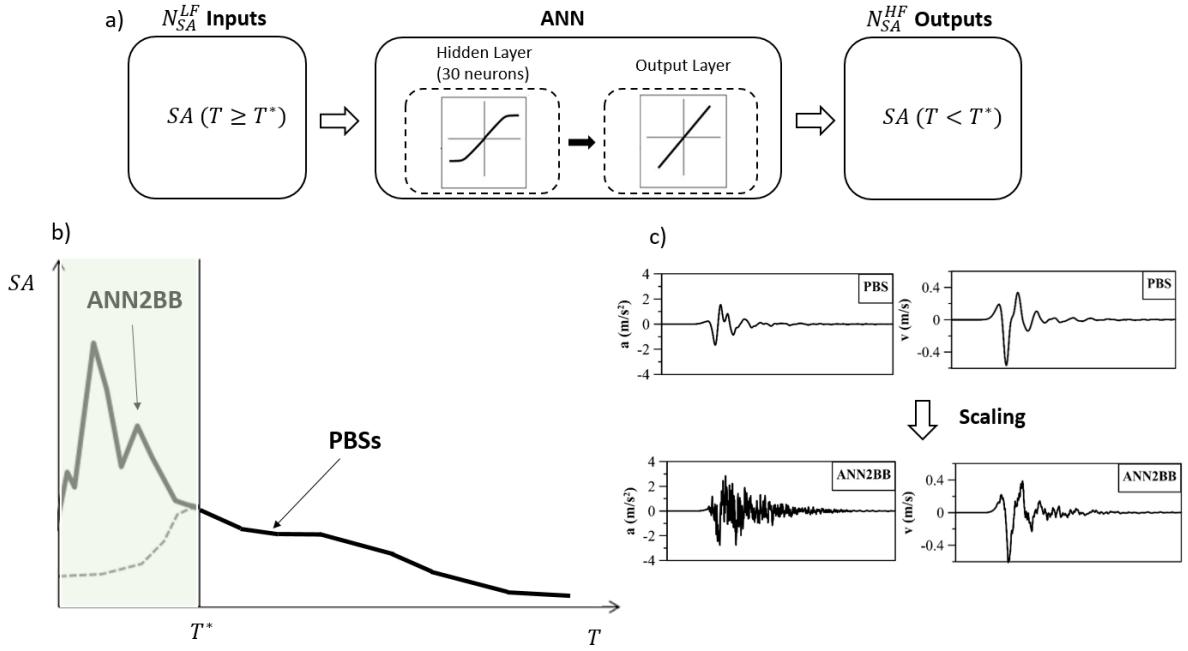

Figure 1 a) Training scheme of the ANN used in this study: the long-period spectral ordinates $SA(T \geq T^*)$, in which T^* is the minimum period of validity of the physics-based numerical model, represent the teaching inputs whereas the short-period ones $SA(T < T^*)$ are the outputs predicted by the ANN; b) example of a broadband spectrum obtained by means of ANN2BB procedure: for a given ground motion, SA at short periods ($T < T^*$) are obtained through ANN while at long period ($T \geq T^*$) by PBS; c) scaling to obtain broadband time histories starting from the LF simulated waveforms. Adapted after [Paolucci et al., 2018b].

3D PHYSICS-BASED NUMERICAL SIMULATIONS

The site-specific physics-based PSHA considered in this work was developed from the set of PBS ground motion scenarios, considering earthquake rupture scenarios of Magnitude ranging from 7 to 7.4 along the ~100 km seismic gap of the North Anatolian Fault (NAF), offshore of Istanbul (Turkey). While for a detailed overview we refer to [Infantino et al. 2020], here we limit ourselves to summarize the main features of the 3D numerical model and the most salient outcomes.

The 3D geological model was constructed combining: (i) the digital elevation and bathymetry model (http://www.cgiar-csi.org); (ii) a horizontally layered deep crustal structure [Gürbüz et al. 2000] and (iii) a 3D shallow geological model of *S* and *P* wave velocities (V_S and V_P) variable both in the horizontal and vertical direction based on the information provided by [Özgül 2011]. A visco-elastic soil model was assumed with a frequency proportional quality factor $Q = Q_0 \cdot f/f_0$, where $Q_0 = V_S/10$ and $f_0 = 1$Hz.

Such a model was then combined with the source model, constructed based on seismotectonic knowledge. The strike-slip NAF portion considered, whose geometrical description was obtained from the GEM (Global Earthquake Model) platform (https://www.globalquakemodel.org/), is located about 20-30 km South-West and South of Istanbul and consists of three main segments extending over a length of ~100 km with a concave shape pointing towards Istanbul (Figure 2). A kinematic source description was applied along the fault in terms of a heterogeneous co-seismic slip distribution combined with a slip source function with initiation time and length depending on the local rupture velocity and rise-time. For this application two kinematic rupture models implemented in SPEED were considered, i.e. the model proposed by [Herrero and Bernard 1994], in which the heterogeneities of the slip distribution are assumed to present a k^{-2} spectral decay in the wavenumber domain, and the one proposed by [Schmedes et al. 2012] and further elaborated by [Crempien and Archuleta 2015] complying with the SCEC validation criteria.

Therefore, the source and soil models were condensed into a spectral element numerical model, shown in Figure 2, covering an area of 165x100 km^2 down to 30 km depth and consisting of hexahedral elements with a fourth order spectral degree selected in order to propagate a maximum reliable frequency of about 1.0 Hz. A minimum value of $V_{s,30}$ of 400 m/s was considered, corresponding to a minimum V_s at ground surface of 250 m/s (Infantino et al., 2020).

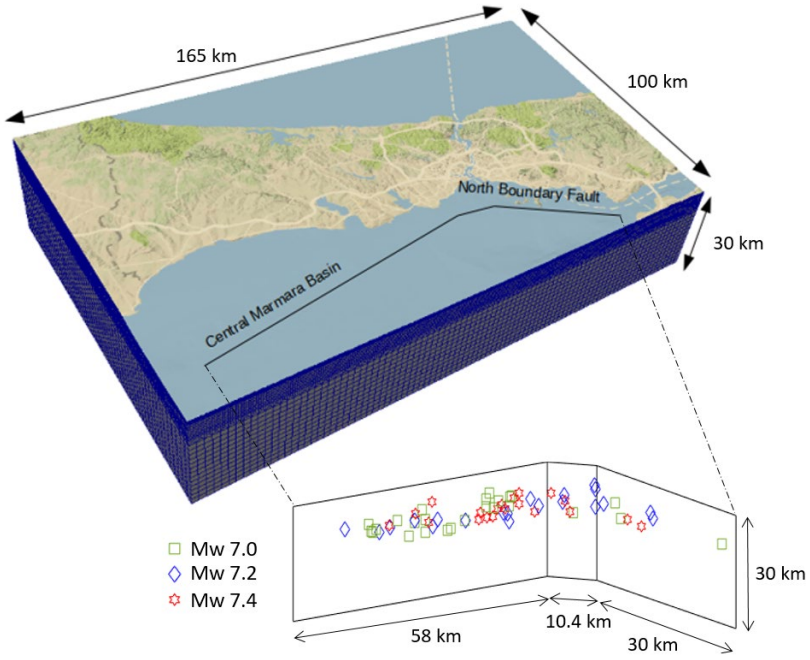

Figure 2 Top: 3D numerical model, the solid line identifies the portion of North Anatolian fault considered in this study consisting of 3 segments; bottom: distribution of the hypocenters of the investigated PBSs along the fault segments.

After verification with an independent numerical solution and after model validation with records of the M_w5.7 earthquake occurred along the Marmara Sea branch of the North Anatolian Fault on Sep 26, 2019, presented elsewhere [Infantino et al., 2020; Stupazzini et al., 2020], a set of 66 PBSs (25 of M_W7.0, 21 M_W7.2 and 20 M_W7.4), with different rupture velocities, mean rise time, depth of the top edge of the active fault and hypocenters distribution, as illustrated in Figure 2, were developed.
The analysis of results revealed as the ground motion levels are controlled by source parameters such as fault geometry, rupture model and directivity phenomena. More specifically, comparison with standard GMPEs showed that, while results for M_W7.0 are in good agreement, as Magnitude increases PBS tend to provide higher amplitudes of ground motion, mostly due to the effect of the geometry of the multi-segment NAF with respect to the city of Istanbul, that enhances the probability of forward directivity pulses in the urban area, as discussed in detail by [Infantino et al., 2020].

STATISTICAL ANALYSIS OF THE 3D NUMERICAL SIMULATION RESULTS

Before integrating the PBSs into the PSHA framework, we addressed two key issues to check the applicability of such results, i.e., (i) whether the number of PBS is sufficient to provide stable estimates of the moments of ground motion and (ii) whether the complexity and variability of kinematic models of slip distribution is sufficient to provide a realistic between-event and within-event variability.

Statistical moments of ground motion

First, we estimated the lognormal distribution of peak ground motion at each site of the study area, together with the number of simulations for each scenario to provide stable measures of the first statistical moments.
As an example, Figure 3 shows, for the Ayasofya site located at some 20 km distance from the NAF and with $V_{s,30}$ around 650 m/s, the histograms of the frequency distribution of simulated horizontal *PGV* and *PGA* values according to the PBSs of M_W7.0 (25 scenarios), 7.2 (21) and 7.4 (20) earthquakes, together with the lognormal distribution fit of the numerical results as well as the corresponding distribution from the CHYO14 [Chiou and Youngs 2014] and BRRM04 [Bray and Rrodriguez-Marek 2004] GMPEs. Note that BRRM04 do not provide predictions in terms of

PGA. For the reasons thoroughly discussed in [Infantino et al. 2020] and shortly mentioned below, this comparison shows that the median predictions from the lognormal distribution (m_y) according to the PBSs (black solid lines) and CHYO14 (black dashed lines) distributions are close for M_W7.0 and 7.2, while they differ substantially for M_W7.4, with the PBSs median (0.46 m/s) twice as large as the CHYO14 (0.23 m/s) but relatively close to the median value predicted by BRRM04 (0.36 m/s).

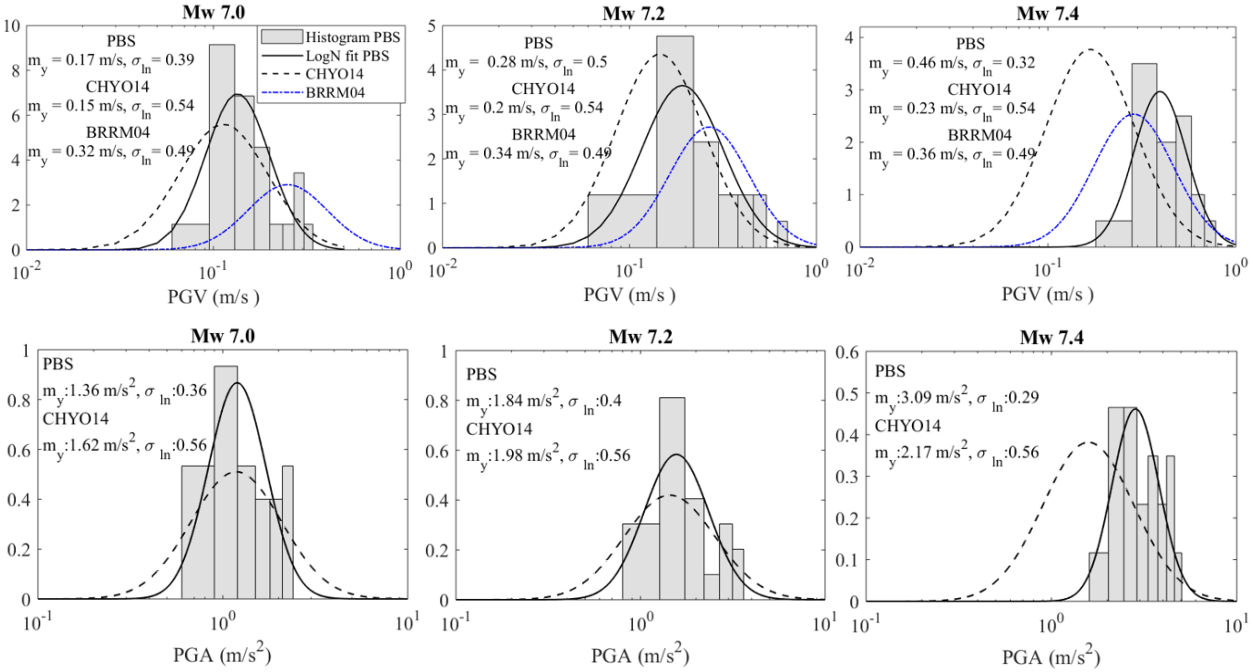

Figure 3 Histogram and lognormal distributions (solid lines) fitting the *PGV* (top) and *PGA* (bottom) simulated in Ayasofya station using the set of PBSs of M_W7.0 (left), M_W7.2 (center) and M_W7.4 (right). For each magnitude, the distributions estimated by CHYO14 (black dashed line) and BRRM04 (blue dashed line) are added, as well as the corresponding values of m_y and σ_{ln} (median and standard deviation, respectively, of the lognormal distribution). Predictions of PGA by BRRM04 are not available.

We also notice that the standard deviation (σ_{ln}) of the lognormal distribution from PBS results is generally smaller than provided by GMPEs, but that it is in reasonably good agreement with the fully non-ergodic values of about 0.4 reported by [Al Atik et al., 2010] for both *PGA* and *PGV*. Furthermore, values of σ_{ln} for *PGA* (driven by the ANN2BB procedure) are slightly less than those of *PGV* (driven by PBS), suggesting that the current version of ANN2BB may slightly underestimate the variability of short period ground motion with respect to the long period numerical simulations.

To throw further light on these results, the values of m_y and of σ_{ln} from PBSs were estimated for the entire region of Istanbul, as shown in Figure 4.

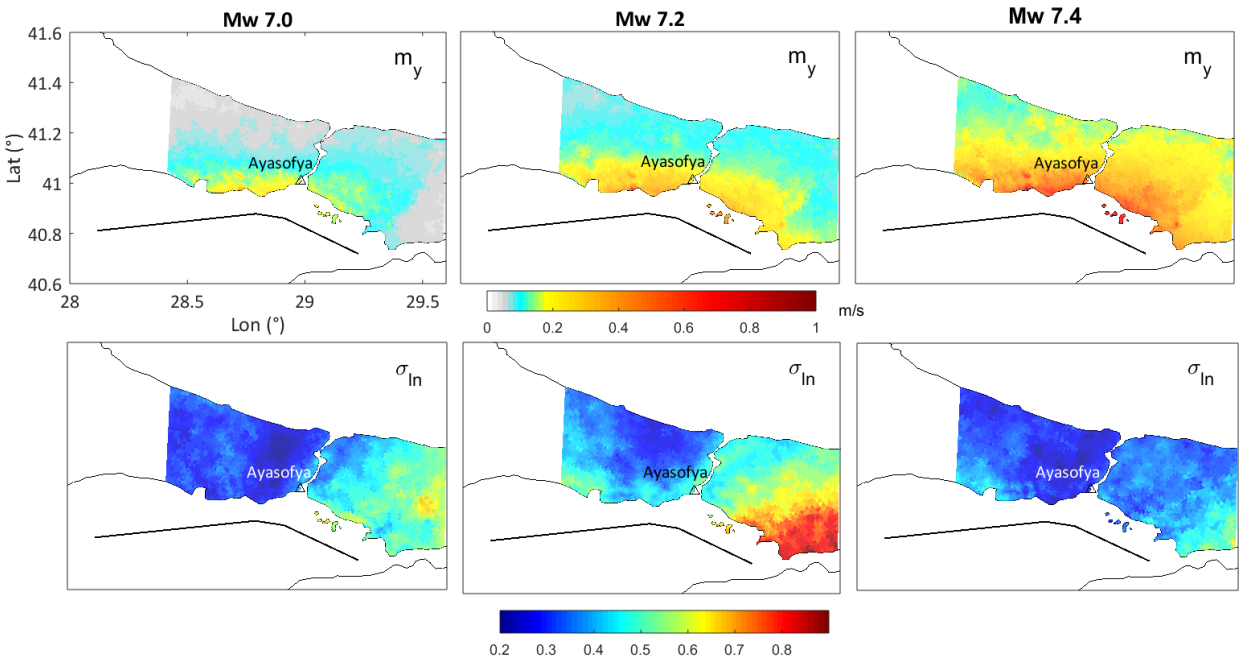

Figure 4 Median (top) and Standard deviation (bottom) *PGV* maps considering the set of scenarios of M_W7.0 (left), M_W7.2 (center) and M_W7.4 (right). The values were obtained assuming a lognormal distribution of the ground motion.

As expected, the largest peak velocity median values occur at short distance from the rupture area, but it is also worth noting that the area subjected to the largest median values (up to about 1 m/s) extends significantly towards the interior of the Istanbul metropolitan area. It is important to remark here that the fault rupture of the M_W7.4 scenarios entirely affects the portion of the NAF segments investigated. In fact, as shown by [Infantino et al., 2020], the convex shape of the NAF in front of Istanbul and its location relative to the megacity are playing a crucial role, enhancing the probability that the realizations of the M_W7.4 scenario present forward directivity effects throughout the urban area of Istanbul (extending both on the East and West side of the Bosphorus Straits). This evidence provides a convincing explanation of the reason why the PBS results fit better the BRRM04 forward-directivity-based GMPE at M_w7.4 rather than CHYO14, while, as magnitude decreases, the conditions for prevailing forward-directivity in Istanbul tend to disappear and PBS results fit much better the CHYO14 predictions.
Moreover, the variability changes significantly as a function of magnitude and of location. As a matter of fact, for a given M_W, the largest values are found at the edges of the fault, probably because of the influence of source rupture directivity. This is suggested by observing the *PGV* variability obtained by the M_W7.2 scenarios Southeast of Istanbul (bottom panel of Figure 4): indeed, depending on the slip distribution and hypocenter location along the fault segments, the area may lie within forward or backward directivity conditions with high event-to-event variability of ground motion.

A key issue to limit the computational effort in the future is to evaluate the minimum number of scenarios required to capture such variability. To this end, we evaluated the stability of the estimates of m_y and σ_{ln} of simulated *PGV*s by making the number of scenarios per magnitude (#PBS) variable from a minimum of 5 up to the total number available (e.g.: for magnitude 7.2 the total number available is 21, therefore $5 \leq$ #PBS ≤ 21). This process was randomly repeated 50 times per each #PBS, creating 50 different permutations with repetition of #PBS scenarios.
Figures 5 shows the mean, standard deviation and min and max values of m_y and σ_{ln} of *PGV* as a function of the number of simulations (#PBS) for each magnitude considered for the Ayasofya site, as shown in Figure 4. Moreover, the corresponding values predicted according the CHYO14 and BRRM04 GMPEs are indicated. It can be inferred that stable estimates of the moments of the lognormal distribution of ground motion can be obtained for a number of simulations equal to about 15, although in some cases such number may even be significantly lower. Although this cannot be considered as a general result, since different effects are not fully explored here (e.g.: average rupture speed variation, fault length and down dip width, rupture progress through the fault bend) it is interesting to note as such values are consistent with the findings of [Villani et al. 2014] who, carrying out a Physics-based PSHA in the Sulmona

area (Italy), by means of statistical analysis found that 15 is the minimum number of PBSs to obtain stable σ_{ln} estimates, while only 5 PBSs were found sufficient to achieve a stable estimate of m_y.

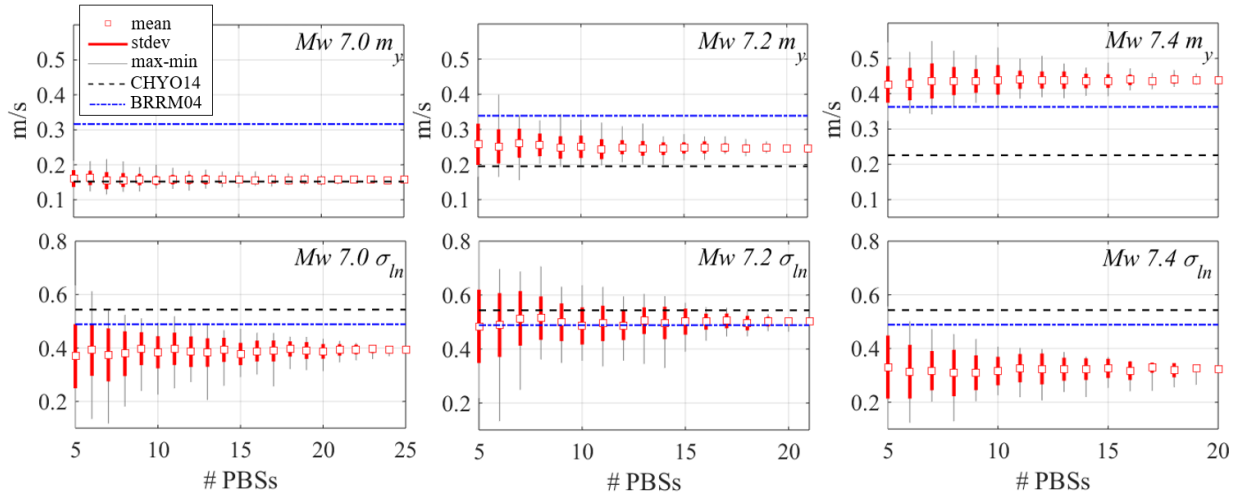

Figure 5 Trend of the median, m_y, and standard deviation (ln), σ_{ln}, as a function of the number of *Mw*7.0, 7.2 and 7.4 PBSs. For each value #PBS, 50 permutations with repetition were randomly selected. The mean (squares), standard deviation (red thick lines) and min and max values (grey thin lines) are shown and compared with the corresponding values predicted according the CHYO14 (black dashed line) and BRRM04 (blue dashed line) GMPEs.

Analysis of between-event and within-event residuals

As a second important test towards applicability of PBS results to PSHA, we verified whether the simulated scenarios provide a realistic picture of the different components of ground motion variability. For this purpose, the analysis of the ground motion residuals from the Istanbul PBSs dataset was conducted.
Following the notation in [Rodriguez-Marek et al. 2011] and denoting by Y_{es} the observed (or simulated) value of ground motion amplitude (logarithm) at station s from event e, by μ_{es} the corresponding predicted value, by δB_e and δW_{es} the between–event and within–event residuals, respectively, we can write:

$$Y_{es} = \mu_{es} + \delta B_e + \delta W_{es} \quad (1)$$

δB_e represents the average misfit, computed among all stations, of the observed ground motion in an individual earthquake e from the median predicted by a GMPE. It is assumed to be a normally distributed random variable with zero-mean and variance τ^2. On the other hand, the within-event residual, δW_{es}, is the misfit between an individual observation at station s and the event-corrected median estimate. It is assumed to be normally distributed with variance $\phi^2_{SS,s}$, where $\phi_{SS,s}$ is generally referred to as the event-corrected single-station standard deviation of the within-event residuals. Knowing $\phi_{SS,s}$ for each individual station s, the event–corrected single station standard deviation ϕ_{SS} of the within-event residuals for the entire dataset can be computed by averaging over all the stations and attributing equal weight to each of them. Then, assuming that δB_e and δW_{es} are statistically independent variables [Rodriguez-Marek et al. 2011], the standard deviation of the total residuals for the entire dataset can be computed as:

$$\sigma_{SS} = \sqrt{\phi_{SS}^2 + \tau^2} \quad (2)$$

Following this procedure, an event-corrected single-station analysis of the standard deviation of Istanbul PBS results was carried out and compared with other published results based both on recorded [Lin et al. 2011, Chen and Faccioli 2013, Villani and Abrahamson 2015] and simulated [Villani and Abrahamson 2015] datasets. More specifically, a

first comparison was made with the findings by [Chen and Faccioli 2013] based on records of the Christchurch seismic sequence, that is one of the very few recorded datasets within an urban area affected by earthquakes with different magnitude but from roughly the same seismic source. The dataset selected by [Chen and Faccioli 2013] consists of 551 records obtained in 65 earthquakes recorded by 14 strong motion stations within the Christchurch area from 2010 to 2012 from events in the Canterbury Plains (New Zealand) with M_W ranging from 4.0 to 7.1, and hypocentral distance from about 10 to 100 km. While [Chen and Faccioli 2013] computed the residuals with respect to the GMPE proposed by [Faccioli et al. 2010], the PBSs residuals of this study were computed with respect to CHYO14. Figure 6 shows the standard deviation components obtained by our PBS results and by [Chen and Faccioli 2013]. Results are in reasonable agreement, considering that they come from two different regions and from datasets of different nature.

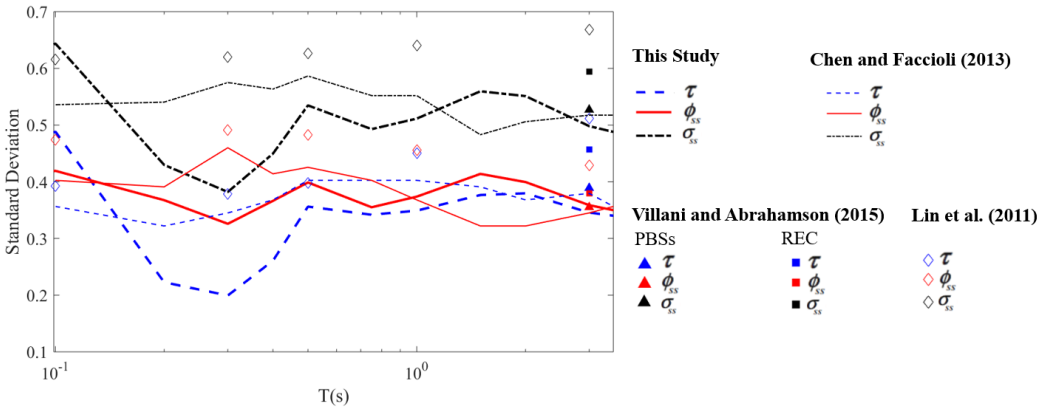

Figure 6 Components of single-station standard deviation of simulations by this study (thick lines), Chen and Faccioli (thin lines) and by [Villani and Abrahamson 2015] (triangle and squares) and [Lin et al. 2011] (diamonds).

Moreover, in Figure 6 the sigma terms obtained by [Lin et al. 2011] and [Villani and Abrahamson 2015] are denoted by markers. More specifically, [Villani and Abrahamson 2015] carried out the analysis for Spectral acceleration (SA) at 3s considering both records (1776 recordings) in Southern California and Cybershake PBSs [Graves et al. 2011] in the Los Angeles Basin (~ 415,000 simulations x 63 sites) while [Lin et al. 2011] performed an analysis on the Taiwan records (4756 recordings from 64 earthquakes and 285 strong motion stations). With few exceptions, these results are in general good agreement, especially in terms of the between-event term τ, revealing as the set of realizations of fault slip distribution considered in our work ensures a realistic variability of earthquake ground motion, in good agreement with the findings from other independent researches.

PHYSICS-BASED SEISMIC HAZARD ASSESSMENT IN ISTANBUL

Physics-based PSHA formulations

In a nutshell, probabilistic seismic hazard assessment (PSHA) at a site can be set in the form:

$$P[IM \geq x] = \sum_{j=1,N} Prob\left[IM > x | scenario_j\right] Prob\left[scenario_j\right] \quad (3)$$

where IM is a parameter of ground motion intensity, x denotes its possible values and N is the number of considered earthquake scenarios. $Prob[scenario_j]$ may typically be given according to a Gutenberg and Richter relationship [Gutenberg and Richter 1944] and the ground motion attenuation model is defined by $Prob\left[IM > x | scenario_j\right]$, which is often provided through a GMPE.

GMPEs are usually developed under the ergodic assumption, according to which the GMPEs can be used at a given site even though they are based on statistical evaluation of datasets of strong motion records from other regions of the world with a similar tectonic framework. However, when using a fully non-ergodic (i.e., site-specific) approach as in

this work, the uncertainty may be strongly reduced, with important implications on the seismic hazard assessment [Abrahamson and Wooddell 2018].

Within a non-ergodic strategy, the term $Prob[IM > x|scenario_j]$ of Equation (3) may be obtained by repetition of PBSs of scenario earthquakes at the site, in a number sufficient for a reliable evaluation of the probability distribution. Although physics-based PSHA provides an obvious advantage to the standard approaches based on GMPEs, as already discussed in the Introduction, there are few examples in the literature of practical applications of such physics-based PSHA. This is mostly because of the large computational efforts required to carry out a sufficiently large number of numerical simulations for a reliable estimate of $Prob[IM > x|scenario_j]$, from low to large magnitude earthquakes. For this reason, it is wise to limit the application of the physics-based PSHA to those contexts where seismic hazard is dominated by few near-source scenarios, from few known seismic fault and/or fault segments, with a relatively narrow range of possible magnitudes.

In this study two approaches are adopted for the application of the physics-based PSHA. The first approach was called *high-resolution* PSHA by [Villani et al. 2014] and consists, for the considered scenario earthquake, of replacing the moments of the lognormal distribution from the GMPE with those obtained from lognormal distribution fitting the frequency histogram of PBSs at each site of interest. This approach was implemented in the CRISIS software [Ordaz et al. 2013] through the so-called *generalized attenuation functions* (GAF).

In the second approach, denoted in this paper as *footprint-based* PSHA, the probability distribution is replaced by the frequency-histogram itself of occurrences of IM values at a given site. This is implemented in practice by averaging, with equal weight, all realizations of the scenario earthquake (Figure 7). In the perspective of seismic hazard assessment alone, i.e. without loss estimations, the main difference of the two approaches is that in the *footprint-based* an upper bound limit for the ground motion distribution is implicitly placed in the PSHA (e.g. McGarr and Fletcher 2007, Bommer et al. 2004, Abrahamson 2000), consisting of the maximum value of the intensity measure among all simulations of the scenario earthquake. On the other hand, when using a GAF approach, a non-zero probability is assigned also to the occurrence of very high (and possibly unrealistic) values of *IM*, with potential impact on the evaluations at very long return periods. In the following, the effect of such difference will be explored on the Istanbul case study.

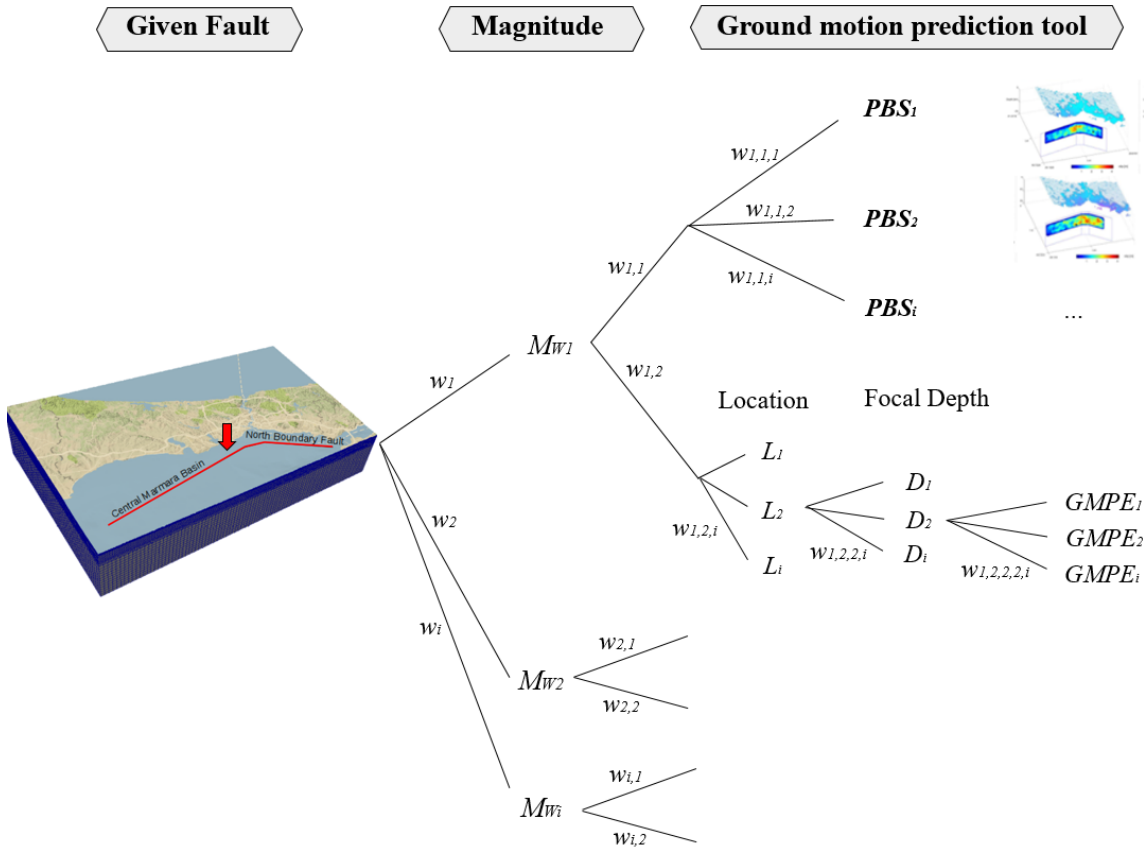

Figure 7 Integration of the PBSs into a classic logic tree approach (M_W: magnitude, L_i: location, D_i: depth, $GMPE_i$: ground motion prediction equation, PBS_i: 3D physics-based scenario, w_i: weight).

APPLICATION TO ISTANBUL

A multiple PSHA in Istanbul was carried out according to the two physics-based PSHA approaches previously outlined, with additional consideration of a standard GMPE-based PSHA, considering the empirical equation of [Chiou and Young 2014], CHYO14, which include a detailed description of the fault, site effects and multiple distance metrics. Of course, even if not considered in the present study, a further mixed approach aiming to incorporate both PBSs and GMPE estimations as different branches of the logic tree would be also possible for the purpose of SHA. To accomplish a consistent comparison, in the GMPE-based PSHA the background seismicity was neglected and the NAF segment shown in Figure 2 was taken as the only seismic source. The occurrence exceedance rates were set equal to $9.1 \cdot 10^{-3}$ y^{-1}, $5.9 \cdot 10^{-3}$ y^{-1} and $4.0 \cdot 10^{-3}$ y^{-1} for M_W7.0, 7.2 and 7.4, respectively, according to representative values in the literature [Sesetyan et al. 2019; Bohnhoff et al. 2016].

For the GAF and GMPE approaches, an integration across the lognormal scatter of the ground-motion distribution (e.g. Bender 1984) up to 3σ was applied, which was found by [Bommer et al. 2004] to provide negligible discrepancies with respect to the whole-range integration down to annual frequencies of exceedance of the order of 10^{-4}.
Figure 8 shows the *PGV* seismic hazard maps using the different PSHA approaches for return periods of 475 years and 975 years. Results from GAF and footprint–based approaches are in good agreement, while they both produce systematically higher results than GMPE-based PSHA especially in the Eastern region and for long return periods, because of the source-directivity effects mentioned previously. Indeed, as discussed in detail by [Infantino et al., 2020], the Eastern side of Istanbul and Prince Islands are the areas mostly affected by forward-directivity (FD) effects, especially for large magnitude.

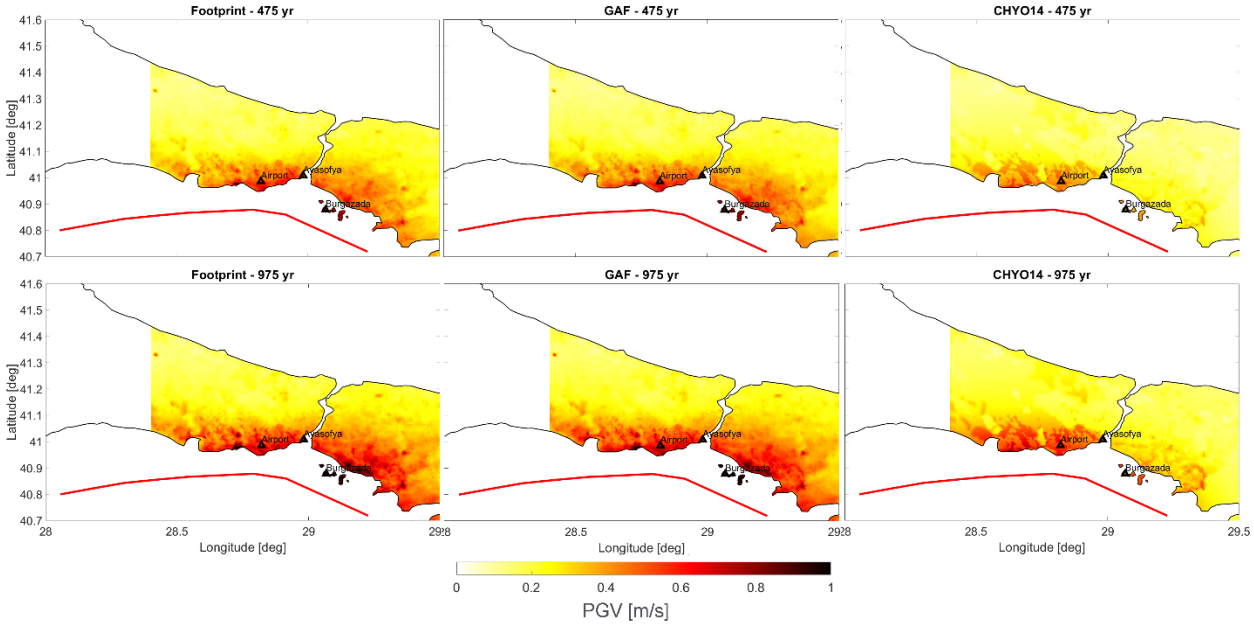

Figure 8 ***PGV*** **Hazard Maps for a return period of 475y (top) and 975y (bottom) according the different PSHA approaches envisaged in this study. From left to right: footprint, GAF and CHYO14 –based PSHA.**

To clarify this point, we also considered PSHA results obtained using the GMPE by [Bray and Rodriguez-Marek 2004], BRRM04, developed to characterize the near-source FD ground motions, and compared them in terms of *PGV* hazard curves (Figure 9) computed for the 3 sites shown in Figure 8 and Figure 11. A clear trend is visible, with the physics-based PSHA results almost bounded on the lower side by the GMPE of CHYO14 and on the upper side by that of BRRM04. At the Airport site, which is seldom affected by FD effects, physics-based results are closer to CHYO14, while at Ayasofya and especially at Burgazada, on the Prince Islands, PBS results get closer to BRRM04. The key role that plays directivity in hazard assessment in Istanbul was highlighted also by [Spagnuolo et al. 2016] who applied the directivity correction factors for long periods developed by [Spudich and Chiou 2008] implementing them in four GMPEs to improve the PSHA in Istanbul. They found that the contribution of rupture directivity leads to an increase of seismic hazard up to 25%, while we found larger values for such an increase, reaching up to about 80% in Burgazada, in the area mostly affected by rupture directivity, in terms of PGV and for annual probability 10^{-3}.

Moreover, it is evident that the footprint hazard curves present an upper bound, because of the truncation to the maximum value, as discussed previously, while the GAF and GMPE hazard curves extend their prediction to very low annual probabilities of exceedance.

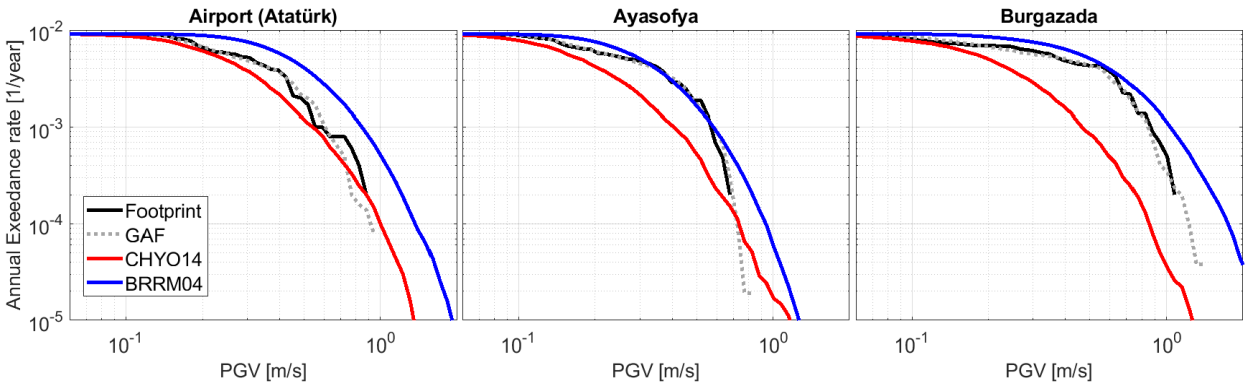

Figure 9 ***PGV*** **Hazard Curves according to the different PSHA approaches considered for three samples sites shown in Figure 8.**

LOSSES CONSIDERING AN ARTIFICIAL PORTFOLIO OF ASSETS

Besides being one of the key ingredients for definition of seismic actions for design, seismic hazard analysis is also preparatory to seismic risk assessment, allowing decision makers to determine the adverse consequences, typically measured in terms of fatalities and/or economic losses, that society might suffer as a result of future earthquakes, and estimating the probability of these consequences for a given time frame.

To highlight the impact of the physics-based PSHA approach outlined in this paper, a simplified comparative probabilistic seismic risk analysis was performed based on GMPE, GAF and footprint. To this end, the three locations in Figure 8 were considered and, for the ease of clarity, it was assumed that a single building typology is present at the selected locations, specifically reinforced concrete low-rise (RC-LR) buildings. Furthermore, in order to disregard the effect of the spatial correlation of the ground motion at scenario level, it was decided to consider three different portfolios, each consisting of assets exclusively located in one of the previously mentioned sites (e.g.: the "Airport (Atatürk)" curves have been computed considering only assets located at that site and nowhere else). For this purpose, we considered the fragility curve proposed by [Özcebe et al. 2014] for RC-LR buildings, that provides the loss ratio, defined as the cost of repair to cost of replacement, as a function of *PGV*. Risk curves, shown in Figure 10, were therefore obtained in terms of Loss Exceedance Curves (LEC) normalized with respect to the Total Sum Insured TSI [Cardona et al., 2008], as typically defined in the (re)insurance industry. As expected, the LEC curves replicate the results obtained in terms of hazard (Figure 9): as a matter of fact, the curves based on GAF or footprint are similar and almost systematically bounded by CHYO14 on the lower side and by BRRM04 on the upper side.

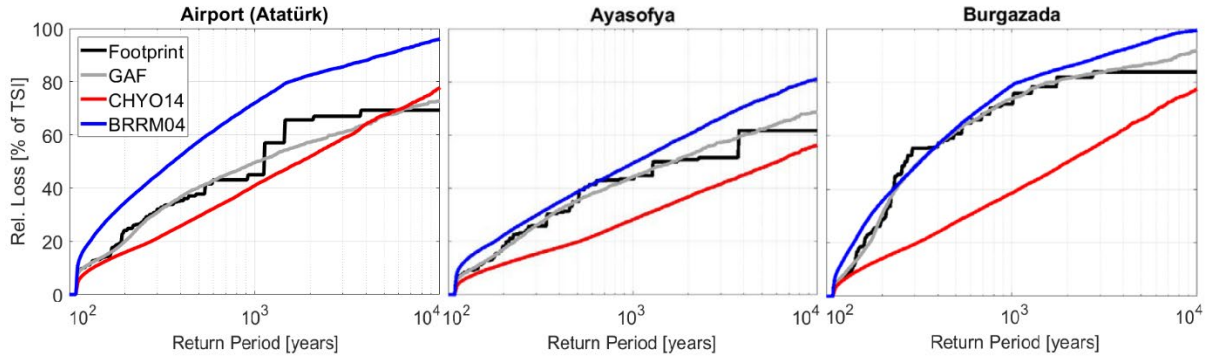

Figure 10 LEC results as function of the return period according to the different PSHA approaches for three representative sites shown in Figure 8 and adopting the Reinforced Concrete (RC) low-rise (LR) vulnerability curve as proposed by Özcebe et al. (2014).

It is worth to remark that the assumption of assets located at a single site at a time implies that the overall losses coincide with the individual loss at each site.

Conversely, the situation changes remarkably once that a set of locations, distributed all over the metropolitan area of Istanbul, is simultaneously considered, as schematically presented in Figure 11 (left). In this case, the spatial correlation of the ground motion plays a crucial role in defining the final loss pattern per scenario. It is worth to remark that both GMPE and GAF -based risk analyses were carried out assuming a distribution of the ground motion truncated at 3σ and, conversely, the footprint-based approach uses directly the PBS simulated in the area.

The LEC curves obtained for a spatially distributed portfolio (Figure 11, right panel) differ now significantly, with the following main features:

- the classical GMPE-based approach shows initially a very steep slope but tends swiftly to a plateau with a maximum expected loss fairly below the one predicted by the other two PBSs methods and by [Bray and Rodriguez-Marek 2004];
- the [Bray and Rodriguez-Marek 2004] loss curve has a shape similar to the one obtained with the standard GMPE even if the losses values are remarkably higher;
- the GAF-based curve (grey continuous line) has a peculiar "step-like" shape, intrinsically related to the limited number of simulated magnitudes. Indeed, independently from the location of the slip pattern along the fault, all scenarios sharing the same magnitude were adopted to calibrate the GAF parameters. Consistently, the spatial correlation existing at scenario level gets lost and the spatial random sampling, adopted in order to reproduce the lognormal distribution of the GAF, is unsuitable to recreate it;
- finally, the footprint-based risk curve is naturally fit to provide realistic loss estimates because each scenario accounts for both: (i) the peculiarity of the near-field wave propagation (e.g. directivity effect) and the (ii) spatial correlation of ground motion. It is worth noting that at around 1000 years return period, the losses estimated with the footprint approach are similar to [Bray and Rodriguez-Marek 2004], due to the similar shaking levels predicted for the M_W7.4 scenario.

In a nutshell, while GAF and footprint-based approaches produce almost identical outcomes in terms of hazard assessment, the second one is highly preferable for risk analysis in large urban areas, unless GAF are supplemented by site-specific spatial correlation models.

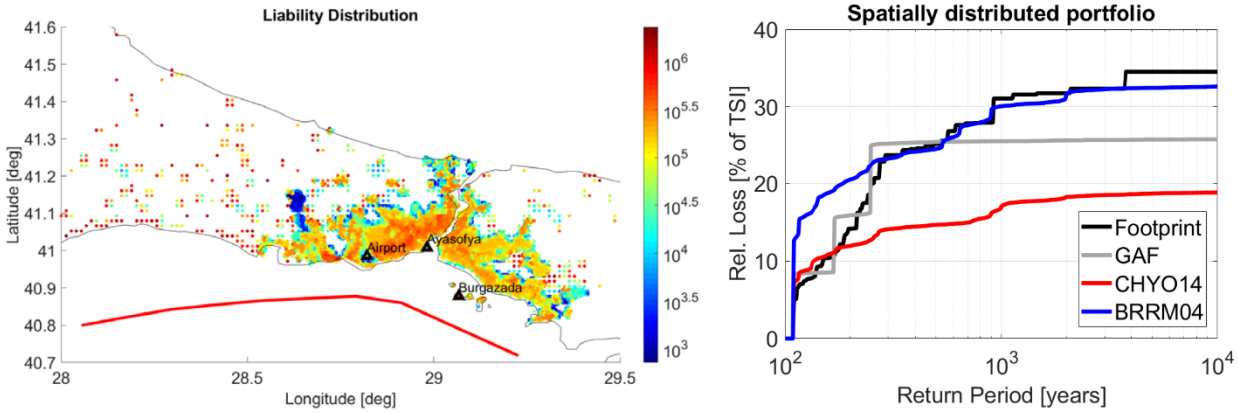

Figure 11 Left: distribution of the insured portfolio within the metropolitan area of Istanbul. Right: LEC curves as a function of the return period according to the different PSHA approaches for a portfolio of assets distributed as presented on the left side and composed only of Reinforced Concrete (RC) low-rise (LR) vulnerability curve as proposed by Özcebe et al. (2014).

DISCUSSION AND CONCLUSIONS

Within an application to seismic loss assessment in Istanbul from earthquakes triggered by the North Anatolian Fault branch crossing the Marmara Sea, we showed the steps needed to carry out a physics-based PSHA and loss assessment including: (i) the creation of a fully 3D physics-based seismic model, verified and validated [Infantino et al., 2020] (ii) the processing of numerical results to produce broadband spectral ordinates, (iii) the detailed check of the simulated ground motions, including a statistical analysis of the entire set of PBSs. The comparison against NGA-W2 GMPE shows a general good agreement for magnitudes 7.0 and 7.2, while large discrepancies have been observed for

magnitude 7.4 scenarios. Differences are explained in terms of prevailing forward directivity conditions towards Istanbul and the comparison with the GMPE by [Bray and Rodriguez-Marek 2004] supports this argument.
More specifically, the present paper puts a special emphasis on the statistical analysis of the broadband synthetics and their use into a PSHA and loss assessment framework. With this objective, the seismic hazard outputs were first illustrated to show the main implications of such an approach, and, secondly, a simplified loss assessment was conducted to quantify the impact of the physics-based PSHA compared to the traditional GMPEs-based approach.
At the end of this work, the advantages and limitations of considering PBSs as an additional tool in support of ground motion modelling for seismic hazard and seismic risk assessment may become clearer. As a matter of fact, we are well aware that our PBS results cannot yet encompass the variability that nature may provide to the complex physics of earthquake source, together with propagation path and local site effects. More particularly, the source parameterization range was limited not only by the high computational costs, but also by the difficulty in attributing a realistic probability of occurrence to several conditions, such as super-shear fault ruptures, although they may be dealt with easily by PBS. In this work we relied on the approach proposed by [Schmedes et al. 2012] as an effective recipe to generate realistic slip distributions complying with the results of dynamic fault rupture models and we proved that the resulting components of ground motion variability are in good agreement with results from literature of fully non-ergodic approaches.
We are also well aware that PBS may not rely on a sufficiently detailed 3D model within a computational domain of tens km of extension. However, the experience gained with the Istanbul case study lead us to conclude that coupling a crustal model with a comprehensive urban microzonation was sufficient to provide a realistic modelling of the area, as confirmed by the successful validation test reported by [Infantino et al., 2020]. Although this may provide satisfactory results for spatially distributed portfolios, a site-specific analysis related to a relevant structure or an industrial facility should account for a more detailed geological information and possibly involve the coupling of PBS results (e.g., at a reference outcropping layer) with a local model.
Having these limitations in mind, it is worth mentioning that the application of PBS to the loss assessment in Istanbul clearly highlighted the key role of forward directivity effects for the M_w7.4 scenario, the occurrence probability of which increases because of the specific location of Istanbul with respect to the NAF and because of the shape itself of the fault. Neglecting such effects, as it would have been done by a standard application of GMPEs, would have led to an underestimation of the epistemic uncertainties and therefore to a substantial underestimation of losses, as shown in Figure 11. Furthermore, while PBSs naturally incorporate the spatial correlation of ground motion, that plays a key role in risk analysis especially when focused for geographically distributed portfolios (e.g.: [Crowley and Bommer, 2006], [Akkar and Cheng, 2016]), GMPEs require a significant effort in order to reproduce it in a reliable way.
We can conclude that integration of verified and validated PBSs within the probabilistic assessment of seismic hazard and seismic risk may provide an excellent complementary tool in support to standard approaches based on GMPEs, especially where the near-fault effects, fault geometry and/or complex 3D geological configurations, not sufficiently constrained by available records, might play a key role. Similar investigations in other urban areas, such as Beijing in China [Infantino et al. 2019; Antonietti et al, 2020] and Christchurch in New Zealand [Stupazzini et al. 2019] confirm the relevance of integrating PBS results into a PSHA, highlighting major variations in the risk evaluations in areas located in the proximity of active faults, especially if such areas are characterized by high population density.
As a final comment to our work we like to quote [Housner 1999]: "*For a large earthquake, the epicenter is not as helpful for engineers as is the footprint*". This sentence, related to the impact of the 17 August 1999 Izmit (Turkey) earthquake has inspired our research and should drive in our opinion future studies with the aim, based on carefully validated and verified PBS approaches, of better understanding and quantifying earthquake ground motion in the near-source region as a key input to enhanced seismic hazard and seismic risk evaluation.

ACKNOWLEDGMENTS

This work has been carried out in the framework of the 2015-2017 research agreement between Munich Re and Politecnico di Milano. Authors are grateful to their co-workers at Politecnico di Milano, Ilario Mazzieri, Chiara Smerzini, Ali Güney Özcebe, for their continuous support during this research. Comments by two anonymous reviewers made possible a significant improvement of the first draft of the manuscript.

REFERENCES

Abrahamson N., and Wooddell K. Probabilistic hazard incorporating 3-D Simulations into nonergodic ground-motion models. Best Practices in Physics-based Fault Rupture Models for Seismic Hazard Assessment of Nuclear Installations: issues and challenges towards full Seismi Risk Analysis, Château de Cadarache, France, 2018.

Abrahamson N. A. State of practice of seismic hazard evaluation. Proceeding, GeoEng2000, Melbourne, Australia, 2000.

Akkar S., Cheng Y., Application of a Monte-Carlo simulation approach for the probabilistic assessment of seismic hazard for geographically distributed portfolio, Earthquake Engng Struct. Dyn. 2016; 45:525–541

Akkar S., Azak T., Çan T., Çeken U., Demircioğlu M. B., Duman T., Erdik M., Ergintav S., Kadirioğlu F.T., Kalafa, D., Kale Ö., Kartal R.F., Kekovalı K., Kılıç T., Özalp S., Poyraz S. A., Şeşetyan K., Tekin S., Yakut A., Yılmaz M. T., Yücemen M. S., and Zülfikar Ö. Evolution of seismic hazard maps in Turkey. Bulletin of Earthquake Engineering 2018; 16:3197–3228.

Al Atik, L., Abrahamson, N., Bommer, J. J., Scherbaum, F., Cotton, F., and Kuehn, N. The variability of ground-motion prediction models and its components. Seismological Research Letters 2010; 81(5):794–801.

Ancheta T. D., Darragh R. B., Stewart J. P., Seyhan E., Silva W. J., Chiou B. S.-J., Wooddell K. E., Graves R. W., Kottke A. R., Boore D. M., Kishida T., and Donahue J. L. NGA-West2 Database. Earthquake Spectra 2014; 30:989-1005.

Ansal A., Akinci A., Cultrera G., Erdik M., Pessina V., Tönük G., and Ameri G. Loss estimation in Istanbul based on deterministic earthquake scenarios of the Marmara Sea region (Turkey). Soil Dynamics and Earthquake Engineering 2009; 29:699 – 709.

Antonietti P. F., Ferroni A., Mazzieri I., Paolucci R., Quarteroni A., Smerzini C., and Stupazzini M. Numerical modeling of seismic waves by discontinuous Spectral Element methods. ESAIM: Proceedings and Surveys 2018, 61:1–37.

Antonietti P. F., Mazzieri I., Melas L., Paolucci R., Quarteroni A., Smerzini C., and Stupazzini M. Three-dimensional physics-based earthquake ground motion simulations for seismic risk assessment in densely populated urban areas. Mathematics in Engineering 2020, Mathematics in Engineering, 3(2): 1–31; doi:10.3934/mine.2021012.

Atakan K., Ojeda A., Meghraoui M., Barka A. A., Erdik M., and Bodare A. Seismic Hazard in Istanbul following the 17 August 1999 İzmit and 12 November 1999 Düzce Earthquakes. Bulletin of Seismological Society of America 2002; 92:466– 482.

Bender B. Incorporating acceleration variability into seismic hazard analysis. Bulletin of Seismological Society of America 1984; 74:1451-1462.

Bishop, C. M. Neural Networks for Pattern Recognition. Clarendon Press, Oxford, United Kingdom 1995.

Bishop C. M., and Roach C. M. (1992). Fast curve fitting using neural networks. Review of Scientific Instruments 1992; 63:4450.

Bommer J. J., Abrahamson N. A., Strasser F. O., Pecker A., Bard P.-Y., Bungum H., Cotton F., Fäh D., Sabetta F., Scherbaum F., and Studer J. The Challenge of Defining Upper Bounds on Earthquake Ground Motions. Seismological Research Letters 2004; 75: 82-95.

Bohnhoff M., Martınez-Garzon P., Bulut F., Stierle E., Ben-Zion Y. Maximum earthquake magnitudes along different sections of the North Anatolian fault zone. Tectonophysics 2016; 674: 147-165.

Boore, D. M. Simulation of ground motion using the stochastic method. Pure and Applied Geophysics 2003; 160(3): 635–676.

Bradley B. A., Razafindrakoto H. N., and Polak V. Ground-Motion Observation from the 14 November 2016 Mw 7.8 Kaikoura, New Zealand, Earthquake and Insight from Broadband Simulations. Seismological Research Letters 2017; 88:740-756.

Bray J. D., and Rodriguez-Marek A. Characterization of forward-directive ground motions in the near-fault region. Soil Dynamics and Earthquake Engineering 2004; 24:815-828.

Cardona O.D., Ordaz M.G., Yamín L.E., Arámbula S., Marulanda M.C. and Barbat A.H. (2008), Probabilistic seismic risk assessment for comprehensive risk management: modeling for innovative risk transfer and loss financing mechanisms, The 14th World Conference on Earthquake Engineering, Oct 12-17, 2008, Beijing, China.

Cauzzi, C., Faccioli, E., Vanini, M., and Bianchini, A. Update predictive equations for broadband (0.01 to 10 s) horizontal response spectra and peak ground motions, based on a global dataset of digital accelerations record. Bulletin of Earthquake Engineering 2015; 13:1587–1612.

Chen. L., and Faccioli E. Single-standard deviation analysis of 2010-2012 strong-motion data from Canterbury region, New Zealand. Bulletin of Earthquake Engineering 2013; 11:1617-1632.

Chiou B. S. J., and Youngs R. R. Update of the Chiou and Youngs NGA Model for the Average Horizontal Component of Peak Ground Motion and Response Spectra. Earthquake Spectra 2014; 30:1117-1153.

Convertito V., Emolo A., and Zollo A. Seismic-Hazard Assessment for a Characteristic Earthquake Scenario: An Integrated Probabilistic-Deterministic Method. Bulletin of the Seismological Society of America 2006; 96:377-391.

Cornell C. A. Engineering seismic risk analysis. Bulletin of Seismological Society of America 1968; 58:1583-1606.

Crempien J. G. F., and Archuleta R. J. UCSB Method for Simulation of Broadband Ground Motion from Kinematic Earthquake Sources. Seismological Research Letters 2015; 86: 61-67.

Crowley H, Bommer JJ. Modelling seismic hazard in earthquake loss models with spatially distributed exposure. Bulletin of Earthquake Engineering 2006; 4(3):249–273.

Erdik M., Demircioglu M., Sesetyan K., Durukal E., and Siyahi B. Earthquake hazard in Marmara region, Turkey. 13th World Conference on Earthquake Engineering, Vancouver, B.C., Canada, 2004.

Esteva L. Criteria for the construction of spectra for seismic design. Proceeding, Third Panamerican Symposium on Structures, Caracas, Venezuela, 1967.

Esteva, L. Bases para la formulación de decisiones de diseño sísmico. Ph.D. Thesis, Universidad Nacional Autonoma de México, Mexico City, México, 1968.

Evangelista L., del Gaudio S., Smerzini C., d'Onofrio A., Festa G., Iervolino I., Landolfi L., Paolucci R., Santo A., and Silvestri F. Physics-based seismic input for engineering applications: a case study in the Aterno valley, Central Italy. Bulletin of Earthquake Engineering 2017; 15:2645-2671.

Faccioli E., Bianchini A., and Villani M. New ground motion prediction equations for T>1s and their influence on seismic hazard assessment. Proceedings, The University of Tokyo Symposium on Long-Period Ground Motion and Urban Disaster Mitigation, Tokyo, Japan, 2010.

Goulet C., Abrahamson N. A., Somerville P. G., and Wooddell K. E. The SCEC broadband platform validation exercise: Methodology for code validation in the context of seismic hazard analyses. Seismological Research Letters 2015; 86:17-26.

Graves R., Jordan T., Callaghan S., Deelman E., Field E., Juve G., Kesselman C., Maechling P., Mehta G., Milner K., Okaya D., Small P., and Vahi K. CyberShake: A Physics-Based Seismic Hazard Model for Southern California. Pure and Applied Geophysics 2011; 168:367-381.

Guidotti R., Stupazzini M., Smerzini C., Paolucci R., and Ramieri P. Numerical study on the role of basin geometry and kinematic seismic source in 3D ground motion simulation of the 22 February 2011 M_W6.2 Christchurch earthquake. Seismological Research Letters 2011; 82:767–782.

Gürbüz C., Aktar M., Eyidogan H., Cisternas A., Haessler H., Barka A., Ergin M., Türkelli N., Polat O., Üçer S. B., Kuleli S., Barıs S., Kaypak B., Bekler T., Zor E., Biçmen F., and Yörük A. The seismotectonics of the Marmara region (Turkey): results from a macroseismic experiment. Tectonophysics 2000; 316:1–17.

Gutenberg B., and Richter C. F. Frequency of Earthquakes in California. Bulletin of Seismological Society of America 1944; 34:185-188.

Herrero A. and Bernard P. A kinematic self-similar rupture process for earthquakes. Bulletin of Seismological Society of America 1994; 84:1216–1229.

Housner G.W. The footprint of an earthquake: opinion paper. Earthquake Spectra 1999; 15:825.

Hutchings L., Ioannidou E., Foxall W., Voulgaris N., Savy J., Kalogeras I., Scognamiglio L., and Stavrakakis G. A. Physically based strong ground-motion prediction methodology; application to PSHA and the M_w = 6.0 Athens earthquake. Geophysical Journal International 2007; 168:659 - 680.

Ince G. Ç. Probabilistic seismic hazard assessment of the historical peninsula of Istanbul. Natural Hazard and Earth System Sciences 2012; 12:3483-3493.

Infantino M., Mazzieri I., Özcebe A. G., Paolucci R., and Stupazzini M. 3D physics-based numerical simulations of ground motion in Istanbul from earthquakes along the Marmara segment of the North Anatolian Fault. Bulletin of Seismological Society of America, published online June 16, 2020, 1-18; doi: 10.1785/0120190235

Infantino M., Mazzieri I., Paolucci R., Allmann A., and Stupazzini M. PSHA incorporating Physics-based Numerical Simulations: the case study of Beijing. 7th International Conference on Earthquake Geotechnical Engineering, Rome, Italy, 2019.

Kalkan E., Gülkan P., Yilmaz N., and Çelebi M. Reassessment of Probabilistic Seismic Hazard in the Marmara Region. Bulletin of the Seismological Society of America 2009; 99:2127-2146.

Kamae K., Irikura K., and Pitarka A. A technique for simulating strong ground motion using hybrid Green's function. Bulletin of Seismological Society of America 1998; 88(2):357–367

Käser M., Morales Aviles W., Bach C., and Stupazzini M. Needs and developments in probabilistic seismic risk assessment for global reinsurance. SECED Conference Earthquake risk and engineering towards a resilient world, Greenwich, London, 2019.

Lin P.-S., Chiou B., Abrahamson N., Walling M., Lee C.-T., and Cheng C.-T. Repeatable source, site, and path effects on the standard deviation for empirical ground-motion prediction models. Bulletin of the Seismological Society of America 2011; 101(5):2281–2295.

Mai P. M., Imperatori W., and Olsen K. B. Hybrid broadband ground-motion simulations: Combining long-period deterministic synthetics with high-frequency multiple S-to-S backscattering. Bulletin of Seismological Society of America 2010; 100(5A):2124–2142.

Mazzieri I., Stupazzini M., Guidotti R., and Smerzini C. SPEED: SPectral Elements in Elastodynamics with Discontinuous Galerkin: a non-conforming approach for 3D multi-scale problems. International Journal for Numerical Methods in Engineering 2013; 95:991–1010.

McGarr A., and Fletcher J. B. Near-fault peak ground velocity from earthquake and laboratory data. Bulletin of the Seismological Society of America 2007; 97:1502-1510.

Mert A., Fahjan Y. M., Hutchings L. J., and Pinar A. Physically based probabilistic seismic hazard analysis using broadband groundmotion simulation: a case study for the Prince Island Fault, Marmara Sea. Earth, Planets and Space 2016; 68.

Motazedian D., and Atkinson G. M. Stochastic finite-fault modeling based on dynamic corner frequency. Bulletin of Seismological Society of America 2005; 95:995–1010

Ordaz M., Martinelli F., D'Amico V., and Meletti C. CRISIS2008: A flexible tool to perform probabilistic seismic hazard assessment. Seismological Research Letters 2013; 84: 495–504.

Özcebe S., Silva V., and Crowley H. Seismic hazard and risk assessment of Turkey. Second European Conference on Earthquake Engineering and Seismology, Istanbul, Turkey, 2014.

Özgül, N. Geology of Istanbul city area (executive summary). Metropolitan Municipality of Istanbul, Directorate of Earthquake & Geotechnical Investigation (in Turkish) 2010. (Turkish version is available online on http://www.ibb.gov.tr/tr-TR).

Paolucci R., Infantino M., Mazzieri I., Özcebe A. G., Smerzini C., and Stupazzini M. 3D Physics-Based Numerical Simulations: Advantages and Current Limitations of a New Frontier to Earthquake Ground Motion Prediction. The Istanbul Case Study. In Recent Advances in Earthquake Engineering in Europe (K. Pitilakis ed.), Geotechnical, Geological and Earthquake Engineering series, Vol. 46, Springer, Chapter 8, 203-223, 2018.

Paolucci R., Gatti F., Infantino M., Smerzini C., Özcebe A. G., and Stupazzini M. Broadband Ground Motions from 3D Physics-Based Numerical Simulations Using Artificial Neural Networks. Bulletin of Seismological Society of America 2018; 108:1272-1286.

Paolucci R., Mazzieri I., and Smerzini C. Anatomy of strong ground motion: near-source records and three-dimensional physics-based numerical simulations of the Mw 6.0 2012 May 29 Po Plain earthquake, Italy. Geophysical Journal International 2015; 203:2001-2020.

Pilz M., Parolai S., Stupazzini M., Paolucci R., and Zschau J. Modelling basin effects on earthquake ground motion in the Santiago de Chile basin by a spectral element code. Geophysical Journal International 2011; 187:929-945.

Razafindrakoto H. N. T., Bradley B. A., and Graves R. W. Broadband Ground-Motion Simulation of the 2011 Mw 6.2 Christchurch, New Zealand, Earthquake. Bulletin of the Seismological Society of America 2018; 108: 2130-2147.

Rodriguez-Marek A., Montalva G. A., Cotton F., and Bonilla F. Analysis of single-station standard deviation using the KiK-net data. Bulletin of the Seismological Society of America 2011; 101:1242–1258.

Roten D., Olsen K., Day S., and Cui Y. Quantification of fault-zone plasticity effects with spontaneous rupture simulations. Pure and Applied Geophysics 2017; 174, 3369-3391.

Schmedes J., Archuleta R. J., and Lavallée D. A kinematic rupture model generator incorporating spatial interdependency of earthquake source parameters. Geophysical Journal International 2012; 192(3):1116–1131.

Şeşetyan K., Demircioğlu M. B., and Akinci A. Evaluation of The Seismic Hazard in The Marmara Region (Turkey) Based on Updated Databases. Geosciences 2019: 9(12): 489

Smerzini C., and Villani M. Broadband numerical simulations in complex near field geological configurations: the case of the M_W 6.3 2009 L'Aquila earthquake. Bulletin of Seismological Society of America 2012; 102:2436–2451.

Spagnuolo E., Akinci A., Herrero A. and Pucci S. Implementing the Effect of the Rupture Directivity on PSHA for the City of Istanbul, Turkey. Bulletin of Seismological Society of America 2016; 106:2599-2613.

Spudich P., and Chiou B. S. J. Directivity in NGA earthquake ground motions: Analysis using isochrones theory. Earthquake Spectra 2008; 24:279-298.

Stupazzini M., Allmann A., Käser M., Mazzieri I., Özcebe A. G., Paolucci R., and Smerzini C. PSHAe (Probabilistic Seismic Hazard Analysis enhanced): the case of Istanbul. Proceedings, 10th Pacific Conference on Earthquake Engineering, Sydney, Australia, 2015.

Stupazzini M., Allmann A., Infantino M., Paolucci R., Smerzini C., Mazzieri I., Guidotti R. and Gardoni P. Footprint based PSHA: The case of Christchurch, New Zealand. 2019 Pacific Conference of Earthquake Engineering, Auckland, New Zealand, 2019.

Stupazzini M., Infantino M., Mazzieri I., Paolucci R., Istanbul, Turkey: verification, validation and scenario simulation by means of physics-based numerical modelling. Submitted to the 17th World Conference on Earthquake Engineering, Sendai, Japan - September 13th to 18th 2020

Taborda R., Azizzadeh-Roodpish S., Khoshnevis N., and Cheng K. Evaluation of the southern California seismic velocity models through simulations of recorded events. Geophysical Journal International 2016; 205:1342-1364.

Taborda R., and Bielak J. Groundmotion simulation and validation of the 2008 Chino Hills, California, earthquake. Bulletin of the Seismological Society of America 2013; 103:131-156.

Taborda R., Bielak J., and Restrepo D. Earthquake groundmotion simulation including nonlinear soil effects under idealized conditions with application to two case studies. Seismological Research Letters 2012; 83:1047-1060.

Tarbali K., Bradley B., Huang J., Lee R., Lagrava D., Bae S., Polak V., Motha J., and Zhu M. Cybershake NZ v18.5: New Zealand simulation-based probabilistic seismic hazard analysis. 7th Conference on Earthquake Geotechnical Engineering, Rome, Italy, 2019.

Villani, M., and Abrahamson, N. A. Repeatable site and path effects on the ground-motion sigma based on empirical data from southern California and simulated waveforms from the Cybershake platform. Bulletin of the Seismological Society of America 2015; 105(5):2681–2695

Villani M., Faccioli E., Ordaz M., and Stupazzini M. High-Resolution Seismic Hazard Analysis in a Complex Geological Configuration: The Case of the Sulmona Basin in Central Italy. Earthquake Spectra 2014; 30:1801-1824.